JPL Publication 12-15

HyspIRI Cloud Mask Detection Algorithm Theoretical Basis Document

G. Hulley
S. Hook
Jet Propulsion Laboratory

National Aeronautics and Space Administration

Jet Propulsion Laboratory
California Institute of Technology
Pasadena, California

Oct 2012

This research was carried out at the Jet Propulsion Laboratory, California Institute of Technology, under a contract with the National Aeronautics and Space Administration.

Revisions:

Version 0.5 draft by Glynn Hulley, 10/01/2012

Edited by JPL docreview, 10/23/2012 (mostly grammatical and wording)

Contacts

Readers seeking additional information about this study may contact the following researchers:

Glynn C. Hulley
MS 183-501
Jet Propulsion Laboratory
4800 Oak Grove Dr.
Pasadena, CA 91109
Email: glynn.hulley@jpl.nasa.gov
Office: (818) 354-2979

Simon J. Hook
MS 183-501
Jet Propulsion Laboratory
4800 Oak Grove Dr.
Pasadena, CA 91109
Email: simon.j.hook@jpl.nasa.gov
Office: (818) 354-0974

Abstract

The Hyperspectral Infrared Imager (HyspIRI) satellite includes a thermal infrared (TIR) multispectral scanner with seven spectral bands in the thermal infrared (TIR) between 7 and 12 µm and one band in the mid-infrared between 3 and 5 µm designed to measure hot targets. The TIR bands have a NEΔT of <0.2 K at 300 K and all bands have a spatial scale of 60 m. The two primary Level-2 products that will be generated by HyspIRI TIR data are land surface temperature and emissivity. A critical aspect of minimizing uncertainties in these products and in generating global Level-3 products is an accurate and reliable cloud mask algorithm. This document describes the methodology behind developing the HyspIRI Cloud Mask Algorithm (HyCMA), and challenges associated with cloud detection. The HyCMA will derive its heritage from previously well established cloud mask algorithms such as the Landsat ACCAA, MODIS MOD35 and AVHRR.

Contents

Figures

Tables

1 Introduction

The Hyperspectral and Infrared Imager (HyspIRI) mission includes two instruments: a visible shortwave infrared (VSWIR) imaging spectrometer operating between 380 and 2500 nm in 10-nm contiguous bands and a thermal infrared (TIR) multispectral scanner with eight spectral bands operating between 4 and 12 μm, both at spatial scales of 60 m. The VSWIR and TIR instruments have revisit times of 19 and 5 days with swath widths of 145 and 600 km respectively. The VSWIR and TIR bands of HyspIRI offer the opportunity for multispectral approaches to cloud detection so that uncertainties from clouds impact quality of the data to a lesser of a degree. However, accurate and reliable cloud detection will be a challenging task for HyspIRI since even though the VSWIR and TIR data will have the same sampling size (60 m), a combination of VSWIR+TIR data will only be available in the VSWIR swath (145 km), and cloud detection for the remainder of the scene will have to rely on TIR data only.

Discriminating clouds is a challenging endeavor and depends on not only the type of cloud being detected, but also the type of surface over which the cloud is detected. Clouds are brighter and colder than the land surface they obscure and these properties can be exploited with the hyperspectral and multispectral characteristics of the HyspIRI VSWIR and TIR instruments. Cloud and land surface variability, however, creates ambiguity in cloud screening. A cloud signature that works well for one scene may be ineffective for another, depending on the land surface type. Accurate cloud identification is also affected by surface features such as snow, ice, and reflective sand that have reflectance signatures similar and in some cases identical to clouds in the visible bands, especially at higher elevations. A scene dependent approach for identifying clouds has been developed for the HyspIRI Cloud Mask Algorithm (HyCMA) and is based on the Landsat Automatic Cloud Cover Assessment (ACCAA) algorithm [*Irish et al.*, 2006]. Other tests developed for the MODIS cloud mask [*Ackerman et al.*, 1998] and AVHRR masks are also employed with HyCMA. Similar to ACCAA, the HyCMA handles the cloud population in each scene uniquely by examining the image data twice. The first pass through the data, Pass One, is designed to capture clouds and only clouds in the VSWIR+TIR swatch (145 km). Eight different filters are used to isolate clouds and to eliminate problem land surface features such as snow and sand. The Pass One goal is to develop a reliable cloud signature for use in Pass Two where the remaining clouds are identified in the remainder of the scene using TIR-only data.

2 HyspIRI Instrument Characteristics

The TIR instrument will acquire data in eight spectral bands, seven of these are located in the thermal infrared part of the electromagnetic spectrum between 7 and 13 μm, and the remaining band is located in the mid infrared part of the spectrum around 4 um. The center position and width of each band is given in Table 1. The exact spectral location of each band was based on the measurement requirements identified in the science-traceability matrices, which included recognition that related data was acquired by other sensors such as ASTER and MODIS. HyspIRI will contribute to maintaining a long time series of these measurements. For example, the positions of three of the TIR bands closely match the first three thermal bands of ASTER, while two of the TIR bands match bands of ASTER and MODIS typically used for split-window type applications (ASTER bands 12–14 and MODIS bands 31, 32). It is expected that small adjustments to the band positions will be made based on ongoing science activities.

The VSWIR instrument will acquire data between 380 and 2500 nm in 10-nm, contiguous bands. The instrument Signal to Noise Ratio (SNR) was modeled for several different input radiances, and these are shown in **Error! Reference source not found.**. The current instrument model includes representative reflectances and transmissions for all surfaces in the instrument optical train. The model also includes the baseline geometry for the instrument and accounts for thermally generated, instrument background photon flux. The read noise and dark current of the sensor is also included. The instrument design minimizes polarization sensitivity and scattered light. The baseline data collection scenario involves observing the land and shallow (<50m) water habitats at full spatial and spectral resolution and transmitting these data to the ground.

In addition, although not driven by the L1 requirements, the VSWIR will provide data over the deep, open ocean. This data will be averaged to a spatial resolution of 1 km and be transmitted to the ground. All data will be quantized at 14 bits. The instrument will have a swath width of 145 km with a ground data sample of 60 m resulting in a temporal revisit of 19 days at the Equator. The nominal overpass time is 10:30 a.m., but this may be adjusted by as much as ±30 minutes to help manage the effects of sunglint on aquatic targets. The absolute radiometric accuracy requirement is greater than 95%, and this will be maintained by using a variety of approaches.

Table 1. Preliminary TIR Measurement Characteristics

Thermal Infrared Measurement Characteristics	
Spectral	
Bands (8) µm	3.98 µm, 7.35 µm, 8.28 µm, 8.63 µm, 9.07 µm, 10.53 µm, 11.33 µm, 12.05 µm
Bandwidth	0.084 µm, 0.32 µm, 0.34 µm, 0.35 µm, 0.36 µm, 0.54 µm, 0.54 µm, 0.52 µm
Accuracy	<0.01 µm
Radiometric	
Range	Bands 2–8 = 200 K–500 K; Band 1= 1200 K
Resolution	< 0.05 K, linear quantization to 14 bits
Accuracy	< 0.5 K 3-sigma at 250 K
Precision (NEdT)	< 0.2 K
Linearity	>99% characterized to 0.1 %
Spatial	
IFOV	60 m at nadir
MTF	>0.65 at FNy
Scan Type	Push-Whisk
Swath Width	600 km (±25.5° at 623 km altitude)
Cross Track Samples	9,300
Swath Length	15.4 km (± 0.7 degrees at 623 km altitude)
Down Track Samples	256
Band to Band Co-Registration	0.2 pixels (12 m)
Pointing Knowledge	10 arcsec (0.5 pixels)
Temporal	
Orbit Crossing	11 a.m. Sun synchronous descending
Global Land Repeat	5 days at Equator
On Orbit Calibration	
Lunar views	1 per month {radiometric}
Blackbody views	1 per scan {radiometric}
Deep Space views	1 per scan {radiometric}
Surface Cal Experiments	2 (day/night) every 5 days {radiometric}
Spectral Surface Cal Experiments	1 per year
Data Collection	
Time Coverage	Day and Night
Land Coverage	Land surface above sea level
Water Coverage	Coastal zone minus 50 m and shallower
Open Ocean	Averaged to 1-km spatial sampling
Compression	2:1 lossless

Table 2. Preliminary VSWIR Measurement Characteristics

Visible Shortwave Infrared Measurement Characteristics	
Spectral	
Range	380 to 2500 nm in the solar reflected spectrum
Sampling	10 nm {uniform over range}
Response	<15 nm (full-width-at-half-maximum (FWHM)) {uniform over range}
Accuracy	<0.5 nm
Radiometric	
Range & Sampling	0 to 1.5 × max benchmark radiance, 14 bits measured
Accuracy and stability	>95% absolute radiometric, 98% on-orbit reflectance, 99.5%
Precision (SNR)	See spectral plots at benchmark radiances
Linearity	>99% characterized to 0.1 %
Polarization	<2% sensitivity, characterized to 0.5 % in sensitive regions
Scattered Light	<1:100 characterized to 0.1% (next nearest neighbor)
Spatial	
Range	>145 km (12 degrees at ~700 km altitude)
Cross-Track Samples	>2400
Sampling	60 m (GSD)
Response	70 m (FWHM)
Uniformity	
Spectral Cross-Track	>95% cross-track uniformity {<0.5 nm min-max over swath}
Spectral-IFOV-Variation	>95% spectral IFOV uniformity {<5% variation over spectral range}
Temporal	
Orbit Crossing	10:30 am sun synchronous descending
Global Land Coast Repeat	19 days at equator
Rapid Response Revisit Cross Track Pointing	3 days (cross-track pointing) 4 degrees in backscatter direction
On Orbit Calibration	
Lunar View	1 per month {radiometric}
Solar Cover Views	1 per week {radiometric}
Surface Cal Experiments	3 per year {spectral & radiometric}
Data Collection	
Land Coverage	Land surface above sea level excluding ice sheets
Water Coverage	Shallow water habitat—50 m and shallower
Solar Elevation	20 degrees or greater
Open Ocean	Averaged to 1-km spatial sampling
Compression	3:1 lossless

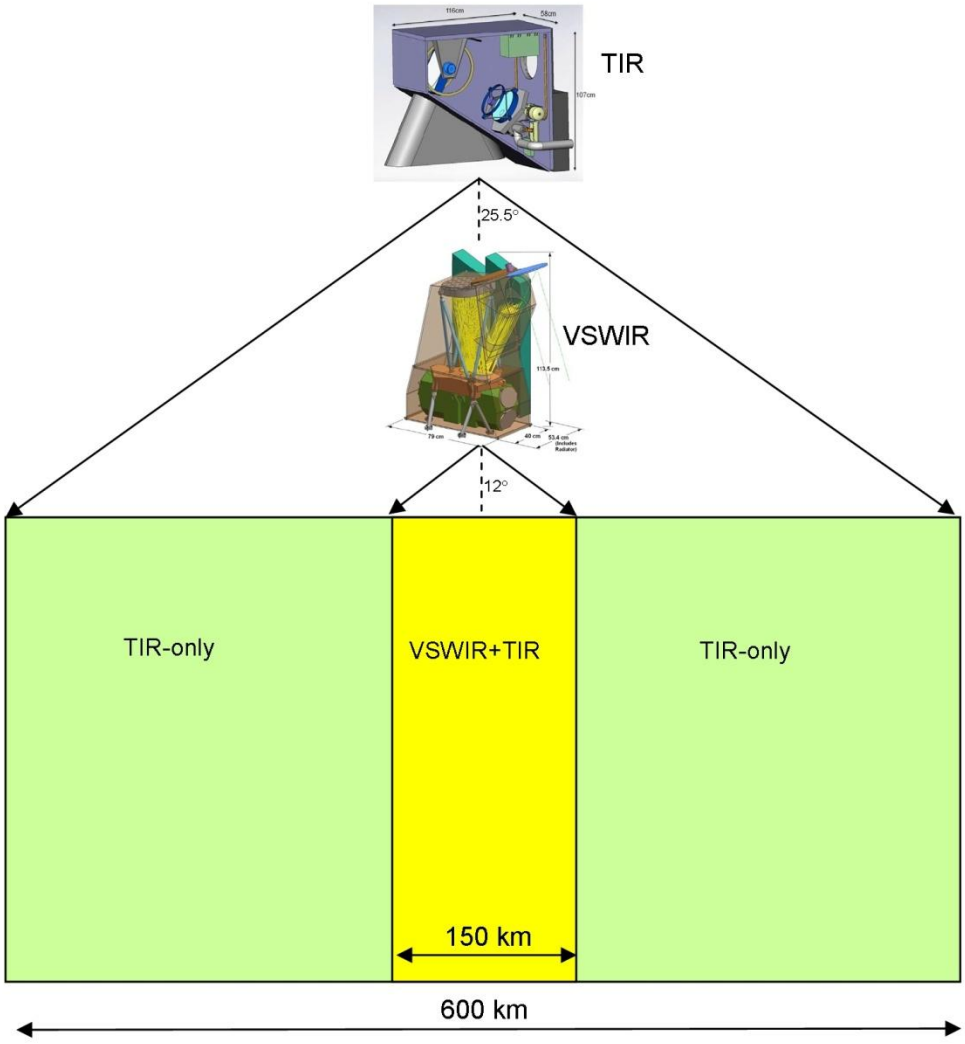

Figure 1. HyspIRI TIR and VSWIR spatial viewing characteristics showing differences between the TIR and VSWIR swaths.

3 Theory and Methodology

3.1 Objectives

The HyspIRI cloud mask indicates whether a given view of the earth surface is unobstructed by clouds or optically thick aerosol. The cloud mask will be generated at 60-m spatial resolution. Input to the cloud mask algorithm is assumed to be calibrated and geolocated level-1B radiance data. The cloud mask will be determined for good data only (i.e., fields of view where data in HyspIRI VSWIR and TIR bands have radiometric integrity). Incomplete or bad radiometric data creates holes in the cloud mask.

Several points need to be made regarding the approach to the HyspIRI cloud mask presented in this Algorithm Theoretical Basis Document (ATBD).

(1) The cloud mask for HyspIRI will be distributed as a separate additional L-2 product, which investigators can use to screen data as appropriate for their studies.

(2) The cloud mask ATBD assumes that calibrated, quality controlled data are the input and a cloud mask is the output.

(3) The snow/ice mask output from the cloud mask output indicates the chosen processing path in the algorithm and should not be considered as confirmation of snow or ice scene. This is the first step in distinguishing cloud from snow in Pass Two of the algorithm.

(4) In certain heavy aerosol loading situations (e.g., dust storms, volcanic eruptions, and forest fires) particular tests may flag the aerosol-laden atmosphere as cloudy. An aerosol and smoke mask will be included in the mask to indicate fields-of-view that are potentially contaminated with optically thick aerosol.

(5) Thin cirrus detection will be output through a separate cirrus mask. The mask is designed to caution the user that thin cirrus may be present, though the cloud mask final result may indicate no obstruction.

There are operational constraints to consider in the cloud mask algorithm for HyspIRI. These constraints are driven by the need to process HyspIRI data in a timely fashion.

- CPU Constraint: Many algorithms must first determine if the pixel is cloudy or clear. Thus, the cloud mask algorithm lies at the top of the data processing chain and must be versatile enough to satisfy the needs of many applications. The clear-sky determination algorithm must run in near-real time, limiting the use of CPU-intensive algorithms. Depending on CPU limitations, the data may be degraded to coarser resolutions for calculating the cloud mask.
- Output Format: Because there are many users of the cloud mask, it is important that the mask not only provides enough information to be widely used, but also that it be easily understood. To intelligently interpret the output from this algorithm, it is important to have the algorithm simple in concept but effective in its application.

In summary, our approach to the HyspIRI cloud mask is, in its simplest form, to provide a binary output (cloudy or clear) for each pixel; and beyond that, to provide additional background information designed to help the user interpret the cloud mask result for his or her particular application, including a snow/ice mask, cirrus mask, and aerosol/smoke mask. The cloud masking algorithm must operate under the following restrictions: near-real time execution, limited computer storage, and simplicity so that many users can follow the algorithm path.

3.2 Background

The Landsat-7 ACCA algorithm employs a rigorous approach for detecting clouds and is based on techniques used by Landsat-4 and 5 and the MODIS cloud mask. The ACCA algorithm uses eight different filters in four bands to distinguish clouds and eliminate problematic land surfaces such as snow and highly reflective desert sands [*Irish et al.*, 2006]. The first pass through a scene uses a spectral analysis to capture cloudy pixels, while a second pass is used to develop a statistical analysis based on the Pass One clouds in order to identify any remaining clouds that were classed as ambiguous in the first pass. The only disadvantage of ACCA is it does not account for cloud shadows and thin cirrus.

The MODIS cloud mask (MOD35) uses 19 channels and 13 threshold-based filters to distinguish clouds [*Ackerman et al.*, 1998; *Ackerman et al.*, 2008]. There are additionally several ancillary data inputs such as a land water map, topography, ecosystems and a snow-ice map. The algorithm is used for a wide variety of applications and provides four levels of confidence with regard to whether a pixel is clear or cloudy; confident clear (99%), probably clear (95%), uncertain clear (66%), and cloudy. The MODIS cloud mask is currently the most sophisticated in terms of the number of spectral tests used and the method of cloud classification [*Ackerman et al.*, 2006; *Frey et al.*, 2008]. The primary drawback is the low resolution of the cloud mask (1 km), which is due to the moderate spatial resolution of the input data.

The development of the MODIS cloud mask algorithm benefited from previous work to characterize global cloud cover using satellite observations from the AVHRR (Advanced Very High Resolution Radiometer) sensor. The International Satellite Cloud Climatology Project (ISCCP) has developed cloud detection algorithms using visible/near-infrared and infrared radiances. The AVHRR Processing scheme Over cLoud Land and Ocean (APOLLO) cloud detection algorithm uses the five visible and infrared channels of the AVHRR, and the NOAA Cloud Advanced Very High Resolution Radiometer 4 (CLAVR) also uses a series of spectral visible and spatial variability tests for cloud detection.

The ISCCP cloud masking algorithm utilizes the narrowband visible (0.6 μm) and the infrared window (11 μm) channels on geostationary platform [*Rossow and Garder*, 1993; *Rossow and Duenas*, 2004]. Observed radiances are compared with corresponding clear-sky values, and clouds are detected only when they alter the clear-sky radiances by more than the uncertainty in the clear values. Using this methodology, cloud detection thresholds are determined by the magnitude of the uncertainty in the clear radiance estimates.

The ISCCP algorithm is based on the premise that the observed visible and infrared radiances are caused by only two types of conditions, cloudy and clear, and that the ranges of radiances and their variability associated with these two conditions do not overlap [*Rossow and Garder*, 1993]. As a result, the algorithm is based upon thresholds; a pixel is classified as cloudy only if at least one radiance value is distinct from the inferred clear value by an amount larger than the uncertainty in that clear threshold value. The uncertainty can be caused both by measurement errors and by natural variability. This algorithm is constructed to be cloud-conservative, minimizing false cloud detections but missing clouds that resemble clear conditions.

The ISCCP cloud-detection algorithm consists of five steps [*Rossow and Garder*, 1993]: (1) space contrast test on a single infrared image; (2) time contrast test on three consecutive infrared images at constant diurnal phase; (3) accumulation of space/time statistics for infrared and visible images; (4) construction of clear-sky composites for infrared and visible every 5 days at each diurnal phase and location; and (5) radiance threshold for infrared and visible for each pixel.

The APOLLO scheme uses AVHRR channels 1 through 5 at full spatial resolution, nominally 1.1 km at nadir [*Saunders and Kriebel*, 1988]. The 5 spectral bandpasses are approximately 0.58–0.68 μm, 0.72–1.10 μm, 3.55–3.93 μm, 10.3–11.3 μm, and 11.5–12.5 μm. The technique is based on five threshold tests. A pixel is called cloudy if it is brighter or colder than a threshold, if the reflectance ratio of channels 2 to 1 is between 0.7 and 1.1, if the temperature difference between channels 4 and 5 is above a threshold, and if the spatial uniformity over ocean is greater than a threshold. These tests distinguish between cloud-free and cloudy pixels. A pixel is defined as cloud-free if the multispectral data have values below the threshold for each test. The pixel is defined as cloud-contaminated if it fails any single test, thus it is clear-sky conservative. Two of those tests are then used with different thresholds to identify cloud-filled pixels from the sub-pixel clouds.

The NOAA CLAVR algorithm (Phase I) uses all five channels of AVHRR to derive a global cloud mask [*Stowe*, 1991]. It examines multispectral information, channel differences, and spatial differences and then employs a series of sequential decision tree tests. Cloud free, mixed (sub-pixel cloud), and cloudy regions are identified for 2×2 global area coverage (GAC) pixel (4-km resolution) arrays. If all four pixels in the array fail all the cloud tests, then the array is labeled as cloud-free (0% cloudy). If all four pixels satisfy just one of the cloud tests, then the array is labeled as 100% cloudy. If 1 to 3 pixels satisfy a cloud test, then the array is labeled as mixed and assigned an arbitrary value of 50% cloudy. If all four pixels of a mixed or cloudy array satisfy a clear-restorer test (required for snow or ice, ocean specular reflection, and bright desert surfaces) then the pixel array is re-classified as

"restored-clear" (0% cloudy). The set of cloud tests is subdivided into daytime ocean scenes, daytime land scenes, nighttime ocean scenes and nighttime land scenes.

Subsequent versions of CLAVR use dynamic thresholds predicted from the angular pattern observed from the clear-sky radiance statistics of the previous 9-day repeat cycle of the NOAA satellite for a mapped one-degree equal-area grid cell. As a further modification, CLAVR will include pixel-by-pixel classification based upon different threshold tests to separate clear from cloud-contaminated pixels and to separate cloud-contaminated pixels into partial and overcast cover. Cloud contaminated pixels are classified as belonging to low stratus, thin cirrus, and deep convective cloud systems. A fourth type indicates all other clouds, including mixed level clouds.

A new cloud mask was recently developed for ASTER termed the New ASTER Cloud Mask Algorithm (NACMA) [*Hulley and Hook*, 2008]. The algorithm was developed by selecting key tests from the Landsat-7, MODIS, and AVHHR algorithms highlighted above. Using this approach a hybrid cloud detection algorithm that capitalized on the previous approaches was developed. For identifying clear-pixels for surface parameter datasets, the cloud mask was designed to be clear-sky conservative (i.e., overestimate rather than underestimate the amount of cloud), and filter threshold values were adjusted to account for this. Additionally, a cloud-filling technique was used to fill in gaps between clouds and shadows. For the HyCMA, a similar approach as NACMA was developed by taking advantage of previous well-reputed algorithms and will be described in the sections that follow.

3.3 Brightness temperature and reflectance calculations

For each HyspIRI observation, the solar zenith angle, sensor zenith and azimuth angle, year, month, day, and radiances for bands 13 (10.6 µm), and 14 (11.3 µm), are computed from the L1B files (geolocated radiance at sensor). Brightness temperatures are calculated on a pixel-by-pixel basis using the formula:

$$T_b(\lambda) = \frac{c2}{\lambda \cdot \ln\left(\frac{c1}{\lambda^5 \cdot \pi \cdot L_\lambda} + 1\right)} \quad (1)$$

where:

λ is wavelength in μm
$c1$ = 0.0143877
$c2$ = 3.741775e-22
L_λ is the at-sensor spectral radiance in $W/(m^2 \cdot sr \cdot \mu m)$

The Top of Atmosphere (TOA) reflectance (planetary albedo), r_λ, is calculated as follows (Markham and Barker, 1986):

$$r_\lambda = \frac{\pi \cdot L_\lambda \cdot d^2}{E_\lambda \cdot \cos\theta} \tag{2}$$

where:

E_λ is the exoatmospheric solar irradiance in $W/(m^2 \cdot \mu m)$ for each spectral band
L_λ is the at-sensor spectral radiance in $W/(m^2 \cdot sr \cdot \mu m)$
d is the Earth-Sun distance in Astronomical Units
θ is the solar zenith angle

The exoatmospheric irradiance is based on the Modtran-3 spectrum computed by Markham and Barker [1986] and is 1554 $W/(m^2 \cdot \mu m)$ at 0.66 µm.

The Earth-Sun distance is computed using the formula:

$$d = \frac{1 - e^2}{1 + e\cos(2\pi(yd - 4)/365.25)} \tag{3}$$

where e is the Earth eccentricity (0.016710219), and yd is the day of year. In AST-JPLv1 brightness temperatures are computed for bands 13 and 14, while reflectance is computed for band 2.

4 Daytime Cloud Tests

The HyspIRI cloud mask will be based on the Landsat ACCAA cloud algorithm as discussed earlier with some modifications. The algorithm has two steps, Pass One and Pass Two. The initial pass, Pass One, through the L1-B image data is designed to isolate clouds in the VSWIR+TIR data overlap. Eight different filters are devised for this purpose based on a combination of VSWIR and TIR data. The Pass One goal is to develop a reliable cloud thermal signature for use in Pass Two where the remaining clouds will be identified in the TIR-only swath. Cloud errors must be minimized as they corrupt the cloud one signature and distort the final cloud cover score. Three category classes result from Pass One processing—clouds, non-clouds, and an ambiguous group that is revisited in Pass Two.

4.1 Pass One Processing

The cloud mask for HyspIRI will be processed on a pixel-by-pixel basis. Filtering is performed on each pixel until it is either classified as clear or cloudy. A description of each filter, presented in the order implemented follows, and is based on Landsat methodology [*Irish et al.*, 2006]. Cloud, clear-sky,

and ambiguous (uncertain) pixels are first classified in Pass One using a combination of visible shortwave infrared (VSWIR) and thermal infrared (TIR) tests and thresholds for the VSWIR/TIR overlapping area of the HyspIRI swath.

4.1.1 Filter 1 – Brightness Threshold

Each 0.65 µm reflectance pixel in the scene is first compared to a brightness threshold initially set to a reflectance value of 0.2. Pixels that fall below this threshold are identified as non-clouds and are flagged as such in the cloud mask. Pixels that exceed the 0.65 µm band threshold, which is set at 0.2, are passed to filter 2. An example of a Landsat-5 0.65 µm reflectance is shown in Figure 2.

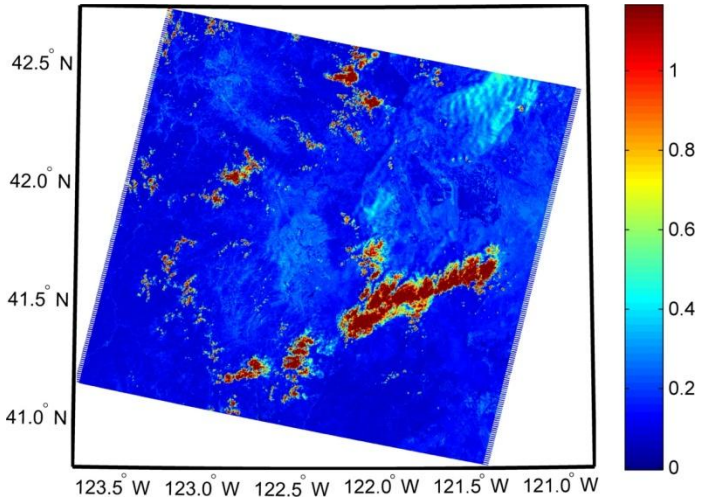

Figure 2. Simulated HyspIRI 0.65 µm band reflectance using Landsat-5 data on 3 July 2004 over Southern California. Clouds show up as areas of high reflectance in red.

4.1.2 Filter 2 – Normalized Snow Difference Index

Pixel values from the 0.55 µm and 1.65 µm reflectances are used to formulate the normalized difference snow index (NDSI). The NDSI filter is expressed as:

$$NDSI = [R(0.55\ \mu m) - R(1.65\ \mu m)] / [R(0.55\ \mu m) - R(1.65\ \mu m)] \quad (4)$$

where R(0.55 µm) is the reflectance for the 0.55 µm channel. This filter is particularly useful for eliminating snow. The reflectance of clouds and snow is similar at 0.55 µm. However, at 1.65 µm, reflectance for clouds is very high while for snow it is low. Hall discovered that NSDI values greater than 0.4 were useful to discriminate between snow/clouds, but clouds composed of ice crystals (e.g., cirrostratus) were also eliminated. The threshold was raised to 0.7 to capture clouds of this type. For HyspIRI, this threshold has been adjusted to 0.65, using sensitivity tests. NDSI values above this threshold qualify as snow and are recorded as non-cloud in the cloud mask. Snow pixels that remain unfiltered are usually found and identified by subsequent filters. Knowledge of snow in a scene is used

in Pass Two processing and the number of snow pixels is retained for this part of the processing. Pixels that fall below the NDSI threshold are passed to filter 3 for additional analysis.

4.1.3 Filter 3 – Temperature Threshold

This filter examines the thermal band 11 µm brightness temperature (BT11), to flag potential cloud pixels. A realistic cloud brightness temperature maximum over land is usually 300 K, but this may change depending on the surface type. To account for temperature changes with elevation, the ASTER Digital Elevation Model (DEM) is used along with a standard lapse rate (6 K/km) to calculate an estimate of the threshold, i.e., if the brightness temperature is greater than 300 K – 6*DEM (km), then it is excluded and labeled as non-cloud in the mask. All pixels with temperature a value less than this are passed to filter 4 for additional analysis. An example of Landsat-5 11µm brightness temperatures is shown in Figure 3.

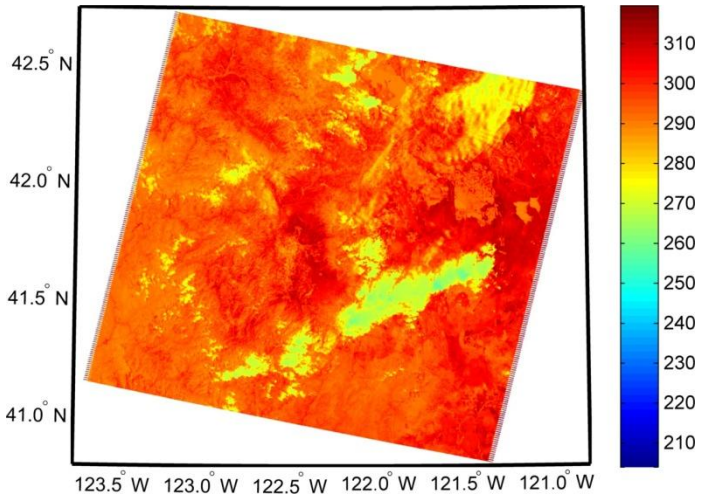

Figure 3. Simulated HyspIRI 11 µm band brightness temperature using Landsat-5 data on 3 July 2004 over Southern California. Clouds show up as areas of lower temperatures in green/yellow.

4.1.4 Filter 4 – SWIR/TIR band Composite

Pixel values from 1.65 µm channel and BT11 are used to formulate the SWIR/TIR Composite. The filter is expressed as:

$$\text{SWIR/TIR composite} = (1 - R(1.65\ \mu m)) * BT11 \quad (5)$$

This filter works exceptionally well because clouds are cold and highly reflective in the 1.65 µm region. It is particularly useful for eliminating cold land surface features that have low 1.65 µm reflectance such as snow and tundra. Sensitivity analysis has demonstrated that a threshold setting of 225 works optimally [*Irish et al.*, 2006]. Pixel values above this threshold are labeled ambiguous in the cloud mask and are revisited in Pass Two. Pixels that fall below this threshold are passed to filter 5.

4.1.5 Filter 5 – NIR/Red Ratio

This filter eliminates highly reflective vegetation and is simply a NIR reflectance (0.8 μm) divided by the red reflectance (0.65 μm). In the near-infrared, reflectance for green leaves is high because very little energy is absorbed. In the red region, the chlorophyll in green leaves absorbs energy so reflectance is low. The NIR/Red ratio results in higher values for vegetation than for other scene features, including clouds. A threshold setting of 2.0 has been used for Landsat ACCAA. Pixels that exceed this threshold are labeled ambiguous and are revisited in Pass Two. Pixels with ratios below this threshold are passed to filter 6.

4.1.6 Filter 6 – NIR/Green Ratio

This filter eliminates highly reflective senescing vegetation and is formed by dividing the NIR (0.8 μm) reflectance by the green reflectance (0.55 μm). In the near-infrared, green leaves that are dead or dying absorb even less energy and are thus highly reflective. In the green region, the leaves absorb less energy because of chlorophyll loss and exhibit increased reflectivity. The NIR/Green ratio values are higher for vegetation than other scene features including clouds. A threshold setting of 2.0 works effectively. Pixels that exceed this number are ambiguous and are revisited in Pass Two. Pixels with ratios below this threshold are passed to filter 7.

4.1.7 Filter 7 – NIR/SWIR Ratio

This filter eliminates highly reflective rocks and sands in desert landscapes and is formed by dividing the 0.8 μm reflectance by the 1.65 μm reflectance. Rocks and sand tend to exhibit higher reflectance at 1.65 μm than at 0.8 μm, whereas the reverse is true for clouds. A threshold setting of 1.0 works effectively. Pixels that fall below this threshold are labeled ambiguous and are revisited in Pass Two. Knowledge of desert pixels in a scene is important for Pass Two processing. Therefore, a desert pixel tally is retained. Pixels with ratios that exceed this threshold are passed to filter 8.

4.1.8 Filter 8 – SWIR/TIR Composite

All pixels reaching this filtering level are classified as clouds. A further separation into two classes is achieved by using the SWIR/TIR composite filter determined from filter 4. For each cloud pixel, the SWIR/TIR composite is compared against a threshold setting of 210. Pixels above and below this threshold are classified as warm and cold clouds, respectively. These two cloud classes are recorded in the cloud mask.

An example ASTER scene is shown in Figure 5 for a distribution of different type of cloud including cumulus and alto-stratus. The HyCMA Pass One was performed on a subset of the middle

portion of this scene to simulate the expected VSWIR/TIR overlap typical of a HyspIRI overpass. The Pass One tests give a good estimate of cloud on the scene when compared to the visible image. Figure 4 also shows the result after each filter test. The results show an increasing accuracy in cloud detection after each filter, starting off cloud-conservative and ending with a more realistic cloud mask.

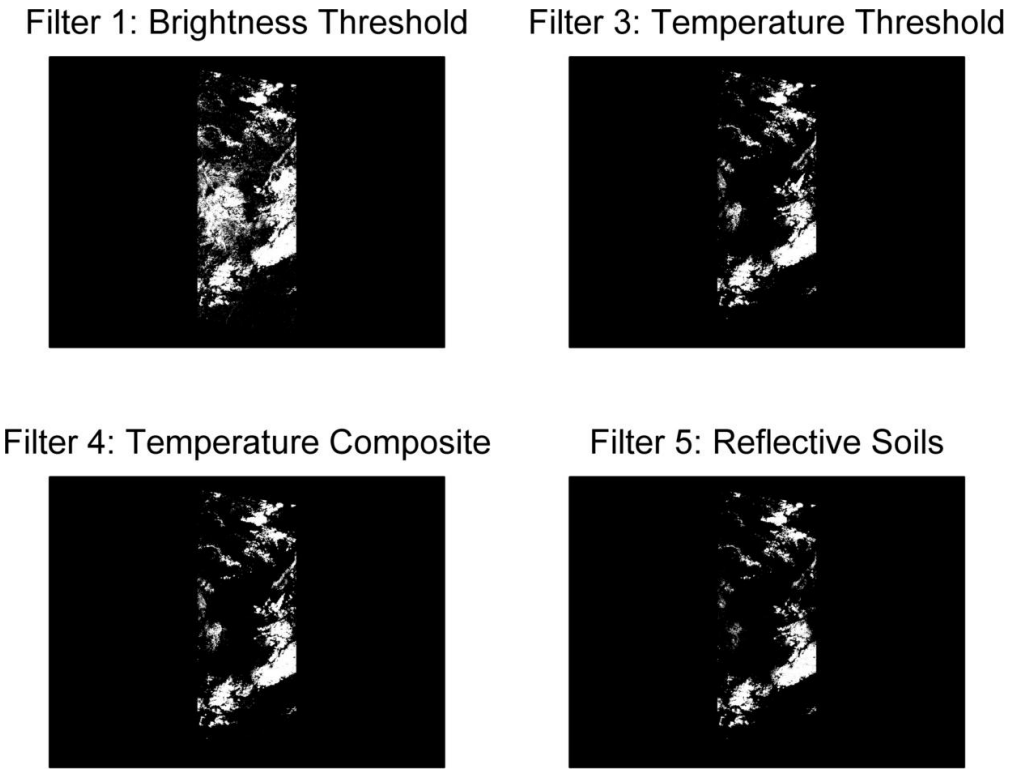

Figure 4. Simulated HyCMA Pass One processing showing results of cloud screening after each of filters 1, 3, 4 and 5 described in section 4.1 for the VSWIR+TIR overlap area. The brightness threshold (filter 1) removes low reflectance pixels, while the temperature threshold (filter 2) removes high temperature pixels. There is no change after filter 4 processing because there was no snow/ice on this scene. Filter 5 further removes highly reflective bare regions (soils, sand, rocks).

4.2 Pass Two Processing

Pass Two processing involves a thermal analysis using the results from Pass One and BT11. A reliable thermal cloud signature is first developed from one or both cloud classes (warm and cold) identified in Pass One, and used to identify if the ambiguous pixels classified from Pass One are clear or cloudy. In addition, all pixels in the TIR-only swath with BT11 temperatures less than 300 K (filter 3) are also classified as ambiguous and examined in Pass Two.

The two classes are combined and used jointly if the scene does not contain snow. Snow creates cloud classification problems and its presence justifies developing a more conservative cloud signature. Snow is determined using filter 2, the NDSI filter. If snow in a scene is less than one percent it is considered snow free. If snow exists in a scene, a more conservative approach is used, and the cold cloud class is used exclusively for rendering the cloud signature. For these scenes the warmer clouds

are relabeled ambiguous and are revisited with all other ambiguous pixels identified during the first pass.

Brightly illuminated bare surfaces (e.g. deserts, semi-arid regions) also create Pass Two processing problems and must be avoided. A desert index is formulated by examining the results of filter 7. The index is computed by dividing the pixel total output from filter 7 by the input pixel quantity. A value of 0.5 or less was found to be a good indicator of terrain with brightly illuminated rocks and sand. Pass Two is bypassed if these land features exist, and the clouds in the remaining TIR-only swath are determined with the BT11 test only (filter 3).

Cloud statistics are computed from either the colder cloud class or the combined group. The cloud population's minimum, maximum, mean, standard deviation, and skewness are computed from the BT11 values. Pass Two processing is engaged if the following three conditions are met: the desert index is greater than 0.5 (the image lacks highly illuminated rocks or sand); the colder cloud population exceeds 0.4 percent of the scene (Pass Two is not required if the scene is cloud free); the mean temperature for the cloud class is less than 295 K (commission errors probably occurred if the mean temperature is this warm). If one or more of these three conditions is breached then thermal analysis is bypassed and processing ends. The colder cloud class from Pass One is used to report the cloud cover percentage for scenes with desert, providing the mean temperature does not exceed 295 K. Otherwise, the scene is considered cloud free.

Pass Two processing requires two new BT11 thresholds against which all ambiguous pixels are compared to. One threshold is set quite low and is used to generate a conservative estimate of clouds in a scene. The other is set high and is used to compute a less restrictive estimate of cloud cover. The thresholds are determined by histogramming the BT11 temperatures for the Pass One cloud population. The histogram's 97.5 and 83.5 percentiles are the starting points for two new temperature thresholds needed for Pass Two.

Threshold adjustments are made if the cloud population skewness is positive. A negative skewness indicates the two thresholds are properly placed at the high end of the temperature range. Consequently, no adjustments are necessary. If skewness is positive, upward adjustments are made to compensate for a warm cloud bias. The shift factor is calculated by multiplying the skewness (the upper limit is held to one) by the standard deviation. Both thresholds are adjusted by this amount. A final check is made to see if the new upper threshold exceeds the histogram's 98.75 percentile (a threshold above or near the cloud temperature maximum is unwanted). If so, the 98.75 percentile

becomes the new upper threshold and the lower threshold is adjusted by the amount of skewness compensation actually allowed.

Processing begins by testing each ambiguous BT11 pixel against the two new temperature thresholds. If a pixel temperature falls below the upper threshold the cloud mask is flagged with a unique number that identifies this class of clouds. This mask value is changed if the pixel temperature also falls below the lower threshold. After BT11 is processed the temperature means and maximums are computed for the two new cloud populations. The percentage of the scene that each cloud class represents is also computed. These two quantities are called the thermal effects.

Analysis of each set of results is performed to determine which thermal effect, if any, to accept. The upper threshold thermal effect is first examined. Commission errors in Pass One distort the cloud signature, resulting in large thermal effects. A thermal effect of more than 40 percent or a mean cloud temperature greater than 295 K is a good indicator that commission errors occurred and an erroneous threshold calculation was made. Under these circumstances, or if snow is present, the upper threshold results are not used. If these three conditions are not breached, the upper threshold results are accepted and the three cloud classes are united in the cloud mask

The conservative thermal effect is examined if the warmer cloud effect is rejected. These results are also dismissed if the thermal effect is greater than 40 percent or if the mean temperature is greater than 295 K. When this happens, the Pass Two analysis is considered invalid and the cloud mask reverts to its Pass One form. The lower threshold results are accepted and the two cloud classes are united in the cloud mask if these conditions are not breached.

Once all ambiguous pixels in the VSWIR+TIR and TIR-only swaths have been analyzed in Pass Two and classified as cloudy or clear, they are combined with Pass One cloudy pixels and the cloud identification process is complete. The final step involves processing the cloud mask for holes. Each non-cloud image pixel is examined and converted to cloud if at least 5 of its 8 neighbors are clouds and holes between clouds are filled in. This operation boosts the cloud cover content to accurately reflect the amount of unusable image data in a scene, and to use a clear-sky conservative approach. At this point, the cloud pixels in the mask are tabulated and a cloud cover percentage score for the scene is computed along with the cloud thermal statistics used in Pass Two.

One possible problem with this method is that it could work for some cloud distributions, but not others. Because the HyspIRI swath will be ~600 km, a classification of the clouds in the VSWIR swath (150 km) in Pass One may not reflect the characteristics and types of the clouds in the remaining

part of the scene. To test this we have applied the HyCMA approach to a combination of ASTER (60 km swath) and Landsat (~400 km swath) data.

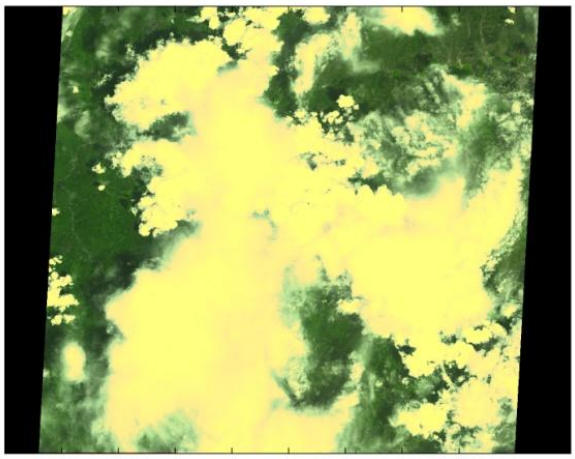

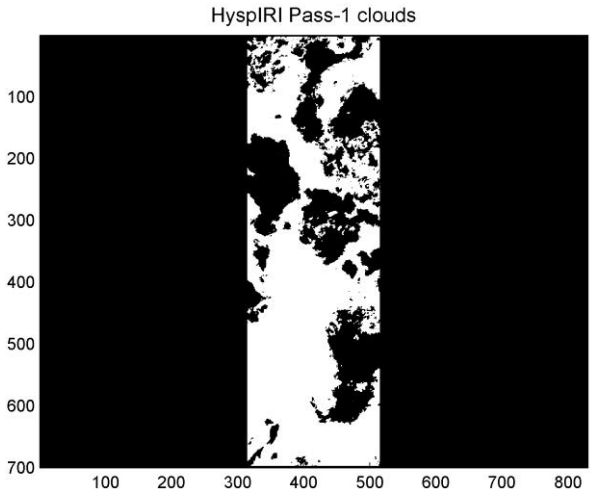

Thermal cloud signature from Pass One	
T mean	252.42 K
Tmax	299.88 K
Tmin	231.52 K
Tsdev	10.7 K
Skewness	0.357
Desert ratio	5.346
Cloud % (pass1)	82.1%
Cloud % (pass2)	85.3%

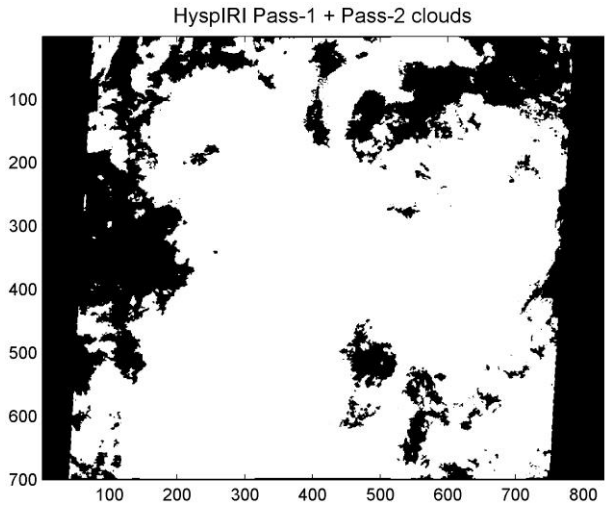

Figure 5. ASTER visible image of a cloud distribution containing a mix of cumulus and altostratus clouds (top left), simulated HyspIRI Pass-One clouds using a combination of VSWIR+TIR data (top right), thermal cloud signature classification using Pass-One cloud statistics (bottom left), and final cloud mask after Pass Two using Pass-One statistics combined with data in the TIR-only portion of the swath.

Figure 5 shows an ASTER false-color visible image with multiple cloud layers consisting of altostratus above a layer of cumulus. This is a difficult case for cloud detection because of the large temperature variation of almost 10 K from one cloud base to the next. This could potentially cause cloud classification errors with filter-4 and Pass Two statistics. Figure 5 (top right) shows a simulated run through Pass One of HyCMA using data from the VSWIR and TIR swath overlap. A thermal signature of these clouds is then developed with the statistics shown in figure 5, and used along with the TIR brightness temperatures to classify the remaining clouds in the scene.

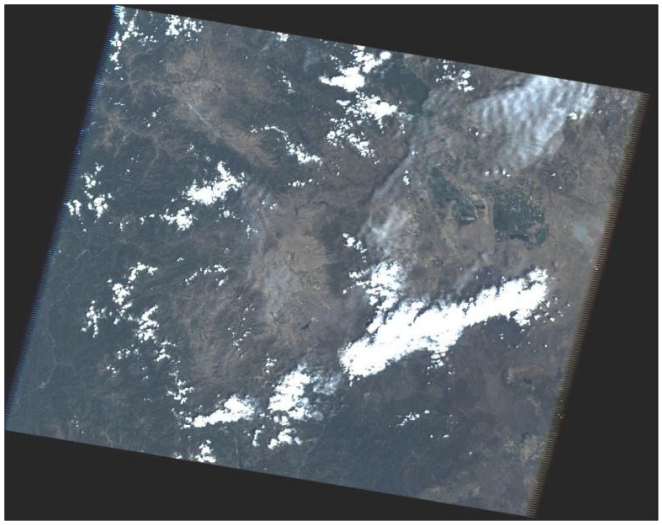

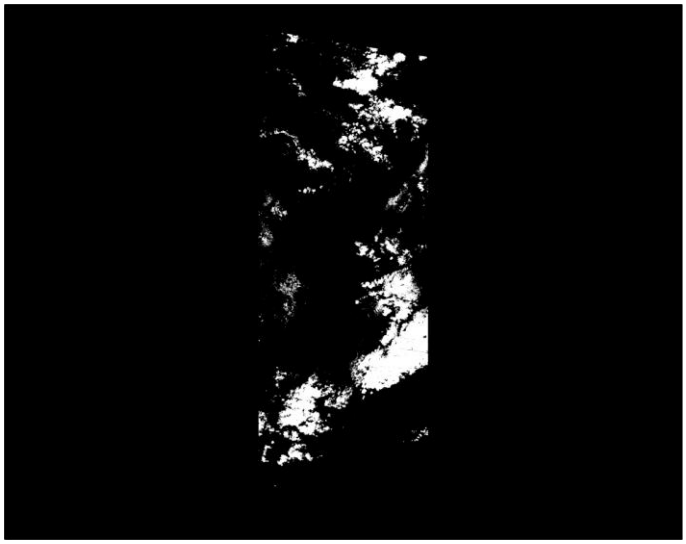

Thermal cloud signature from Pass One	
T mean	275.17 K
Tmax	296.17 K
Tmin	259.46 K
Tsdev	6.66 K
Skewness	0.499
Desert ratio	7.846
Cloud % (Pass One)	14.1%
Cloud % (Pass Two)	19.1%

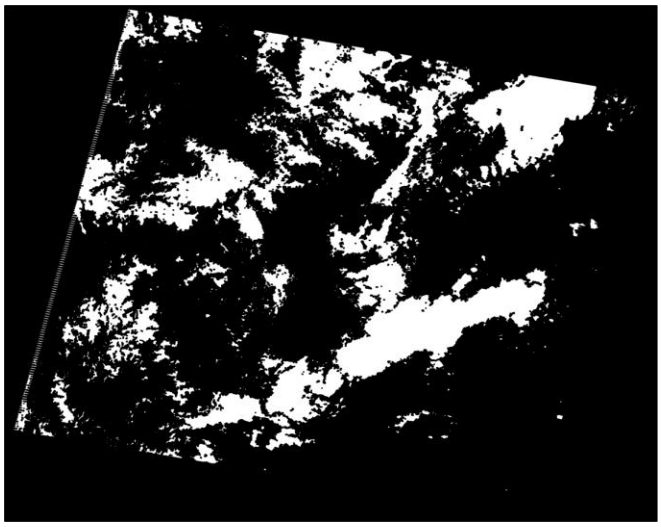

Figure 6. Landsat visible image of a cloud (top left), simulated HyspIRI Pass-One clouds using a combination of Landsat VSWIR+TIR data (top right), thermal cloud signature classification using Pass-One cloud statistics (bottom left), and final cloud mask after Pass Two using Pass-One statistics combined with data in the TIR-only portion of the swath.

Figure 6 shows an example of HyCMA applied to a Landsat 5 scene over southern California with a swath width of 400 km. For this case it is clear that the HyCMA approach works well for larger swaths of data and the clouds have been accurately identified over all parts of the scene. For this case, the pass-two clouds were identified by using the warmer cloud class identified from Pass One. The clouds had a positive skewness as in figure 5 and a shift factor was used to adjust for a possible warm cloud bias as described in section 4.2.

5 Nighttime Tests

A combination of solar zenith angle and instrument mode (day or night mode) at the pixel latitude and longitude at the time of the observation will be used to determine if a daytime or night-

time cloud-masking algorithm should be applied for HyspIRI data. The HyCMA daytime algorithm, which includes VSWIR data, will be constrained to solar zenith angles less than 85°. Nighttime cloud detection is a challenging task since only thermal data is available; however, overland thermal homogeneity at night results in easier application of the thermal brightness temperature test. Other conditions, such as low stratus at night, or the presence of ice/snow make nighttime cloud detection difficult because of the limited contrast with the surface radiance. For these types of conditions, a shortwave channel (e.g., 4 μm) is essential for discriminating clouds from surface features. The following sections describe cloud tests used and employed for nighttime data for the MODIS standard cloud mask, and will be applicable to the HyspIRI mission.

5.1 The 11 μm brightness temperature (BT11) threshold test

This test is identical to the daytime BT11 test (filter 3 in section 4.1.3) and takes advantage of the fact that clouds are cooler than the land/ocean surface. This test is most effective for cold clouds over ocean, and should be used with caution over land due to varying surface emittance. For MODIS data, thresholds are set to 270 K for ocean and 297.5 K for land. This test can also be used as a clear-sky restoral test.

5.2 The 11-3.9 μm brightness temperature difference low cloud test

HyspIRI thermal band 1 will measure radiances in the window region near 3.8-4 μm primarily used for fire detection and temperature estimation. However, this band will also be useful in that differences between BT11 and BT3.9 can be used to detect the presence of clouds. At night, the difference between the brightness temperatures measured in the shortwave (3.9 μm) and in the longwave (11 μm) window regions (BT11 – BT3.9) can be used to detect partial cloud or thin cloud. Small or negative differences are observed only for the case where an opaque scene (such as thick cloud or the surface) fills the field of view of the sensor. Negative differences occur at night over extended clouds due to the lower cloud emissivity at 3.9 μm. During the daylight hours the difference between BT11 and BT3.9 is large and negative because of reflection of solar energy at 3.9 μm. This technique is very successful at detecting low-level water clouds.

Moderate to large differences between BT11 and BT3.9 result when a non-uniform scene (e.g., broken cloud) is observed. The different spectral response to a scene of non-uniform temperature is a result of Planck's law. The brightness temperature dependence on the warmer portion of the scene increasing with decreasing wavelength (the shortwave window Planck radiance is proportional to temperature to the thirteenth power, while the longwave dependence is to the fourth power).

Differences in the brightness temperatures of the longwave and shortwave channels are small when viewing mostly clear or mostly cloudy scenes; however, for intermediate situations the differences become large (greater than 3°C).

The application of BT11–BT3.9 is difficult over deserts during daytime. Bright desert regions with highly variable emissivities tend to be incorrectly classified as cloudy with this test. The problem is mitigated in the MODIS cloud mask somewhat by making use of a double-sided test where brightness temperature differences greater than a "low" threshold but less than a "high" threshold are labeled clear while values outside this range are called cloudy. This threshold strategy along with the use of clear-sky restoral tests is effective for detecting low-level clouds over deserts.

5.3 The 11-12 μm brightness temperature difference cirrus test

The thin-cloud/cirrus test utilizes a brightness temperature difference test between two longwave thermal bands (e.g., 11 and 12 μm) and works well for thin cirrus, the edges of thicker cloud, low reflectance clouds and a variety of other types of cloud. Differences between BT11 and BT12 are widely used for cloud screening with AVHRR and GOES measurements, and this technique is often referred to as the split window technique. *Saunders and Kriebel* [1988] used BT11–BT12 differences to detect cirrus clouds—brightness temperature differences are larger over thin clouds than over clear or overcast conditions and arise due to the different emissivities of the cloud at the two wavelengths as a result of the non-linear nature of the Planck function. In the MODIS cloud mask, thresholds were set as a function of satellite zenith angle and the BT11 brightness temperature.

In the ASTER cloud mask algorithm [*Hulley and Hook*, 2008], the thresholds are computed by looking at BT11–BT12 differences for a variety of clear-sky scenes over varying terrain features including desert, mountainous terrain, and vegetation. For clear sky conditions, the differences should be less than 1 K, but could be as large as 6 K for cloudy conditions. The maximum differences are then noted and used to set appropriate thresholds. For a pixel with given BT11, BT differences greater than the threshold values are classified as cloud. A similar procedure will be used for HyspIRI

Figure 6 is an example of a theoretical simulation of the brightness temperature difference between 11 and 12 μm versus the brightness temperature at 11 μm, assuming a standard tropical atmosphere [*Ackerman et al.*, 2006]. The difference is a function of cloud optical thickness, the cloud temperature, and the cloud particle size distribution. The difficulty in using these tests for cloud detection is often defining the clear-sky value on this type of diagram. Table 3 shows example thresholds based on figure 6 for the MODIS cloud mask algorithm [*Ackerman et al.*, 2006]. HyspIRI

thresholds will be estimated using a variety of different simulations over different land surfaces and similar results from Figure 6.

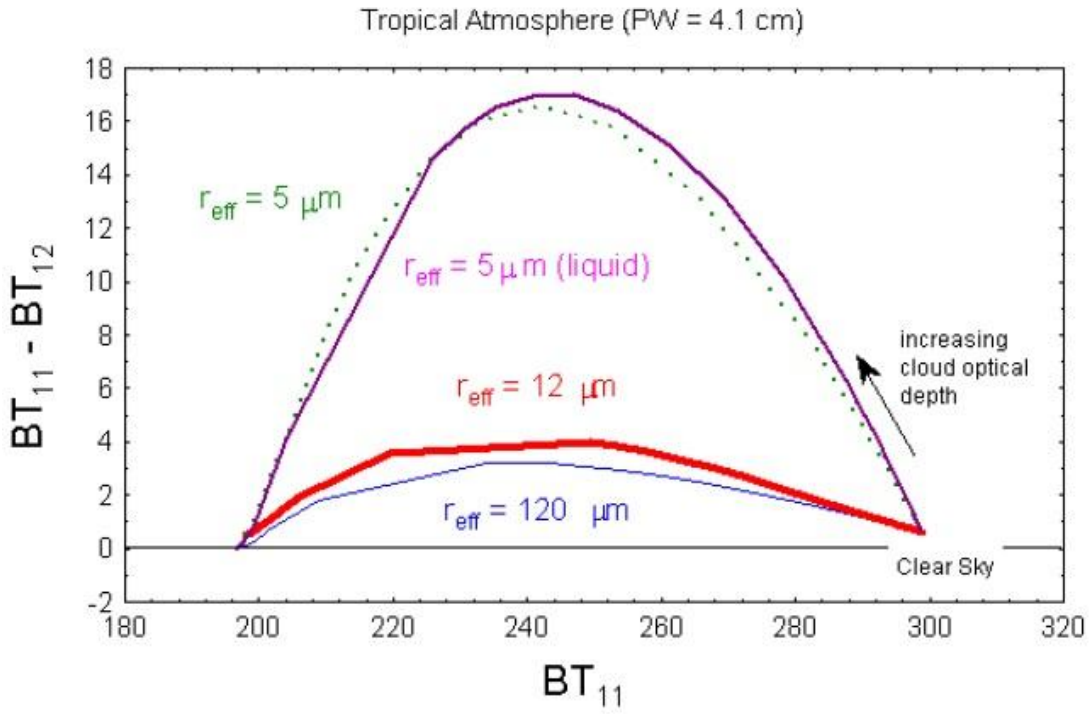

Figure 7. Theoretical simulations of the brightness temperature difference as a function of BT11 for a cirrus cloud of varying cloud microphysical properties (image from *Ackerman et al.*, 2006).

Table 3. Example thresholds used for BT11 threshold test in MOD35 (*Ackerman et al.*, 2006).

Scene Type	Threshold	High confidence clear	Low confidence clear
Day ocean	270 K	273 K	267 K
Night ocean	270 K	273 K	267 K
Day land	297.5 K	302.5 K	NA
Night land	292.5 K	297.5 K	NA
Night desert	292.5K	297.5 K	NA
Day Desert	292.5K	302.5 K	NA

5.3.1 The 3.9-12 μm brightness temperature difference high cloud test

This window brightness temperature difference test is applied during the nighttime over some, but not all, surfaces. This difference is useful for separating thin cirrus and cloud-free condition, and is relatively insensitive to the amount of water vapor in the atmosphere [*Hutchison and Hardy*, 1995]. This test is executed over land at night. The three thresholds for MODIS are 15, 10, and 5 K, for low confidence, mid-point, and high confidence, respectively. Over snow-covered surfaces, the thresholds are adjusted to 4.50, 4.00, and 3.50 K.

Since no satellite data currently exist to simulate a HyspIRI 3.9 μm channel at 60 m resolution, data from MASTER airborne flights will be used to estimate initial threshold limits for this test.

5.3.2 The high cloud 7 μm brightness temperature test

In clear-sky situations, the ~7 μm radiation measured by satellite instruments is emitted by water vapor in the atmospheric layer between approximately 200 and 500 hPa [*Soden and Bretherton*, 1993] and has a brightness temperature (BT7) related to the temperature and moisture in that layer. The 7 μm radiation emitted by the surface or low clouds is absorbed in the atmosphere above and is generally not sensed by the satellite instruments. Therefore, thick clouds found above or near the top of this layer have colder brightness temperatures than surrounding pixels containing clear skies or lower clouds.

Detection of clouds over polar regions during winter is difficult. Under clear-sky conditions, strong surface radiative temperature inversions often exist. Thus, IR channels whose weighting function peaks low in the atmosphere will often have a larger BT than a window channel. For example, BT8.6 > BT11 in the presence of an inversion. The surface inversion can also be confused with thick cirrus cloud; this can be mitigated by other tests (e.g., the magnitude of BT11 or the BT11–BT12). Analysis of BT11–BT6.7 has shown large negative differences in winter over the Antarctic Plateau and Greenland, which may be indicative of a strong surface inversion and thus clear skies [*Ackerman*, 1996]. Under clear-sky conditions, the measured 11 μm radiation originates primarily at the surface, with a small contribution by the near-surface atmosphere. Because the surface is normally warmer than the upper troposphere, BT11 is normally warmer than the 7 μm brightness temperature; thus the difference, BT11–BT7, is normally greater than zero. Large negative differences in BT11–BT7 (less than −10 K) exist over the Antarctic Plateau and Greenland during their respective winters and are indicative of clear-sky conditions and the existence of strong low-level temperature inversions.

6 Validation

For validation of the HyspIRI cloud mask, once enough data is acquired, several difficult-case-scenario scenes will be chosen over different land cover types and for a variety of cloud types. A visual cloud cover assessment (VCCA) will be the primary tool for evaluating the quality of the cloud mask, supplemented by a statistical approach for assessing the total cloud cover on each scene.

6.1 Cloud mask validation strategies

Following the first few years of Landsat 7 operations, the Landsat Project Science Office (LPSO) staff undertook a validation of all elements of the Long-Term Acquisition Plan (LTAP) including the ACCA algorithm [*Markham and Barker*, 1986]. The approach chosen to validate Landsat

ACCA performance, and which we will use for HyspIRI, is a supervised classification of a stratified sample of global scenes using three-band (R,G,B) browse imagery for comparison to corresponding HyCMA cloud mask outputs. For Landsat, B5, B4, and B3 were used to define the red (R), green (G), and blue (B) elements respectively for the browse images. A linear contrast stretch was applied to each browse image to ensure adequate contrast in the RGB product. A reduced-resolution browse-scene approach to assessing cloud cover (CC) is feasible because both ACCA and HyCMA will output a single cloud scene percentage for the entire scene. Furthermore, the ACCA definition of clouds as nearly opaque and the ability to visually compare the supervised classification of browse imagery to adjacent scenes and other dates allowed an iterative and precise analysis approach. This VCCA will be used as a measure of the true CC in the scene.

6.2 Visual cloud-cover assessment (VCCA) validation procedure

Supervised classification will be performed using a procedure described in [*Irish et al.*, 2006]. Calculations will be performed using Adobe® Photoshop® image processing software. The *magic wand* and *freehand lasso* tools of Photoshop® will be used to isolate clouds in the respective RGB browse images. The wand employs a seed-fill threshold algorithm to compute regions of brightness similarity based on a mouse click of a single pixel. The algorithm compares the selected pixel's brightness values to all other pixels and retains those within a selectable tolerance threshold. For example, clicking on an RGB-browse-image pixel with values R:200, G:220, and B:240 and a tolerance set to 5, results in selection of pixels in the ranges: $195<R<205$, $215<G<225$, and $235<B<245$. Additional cloud pixels will be added by using the wand repeatedly until the cumulative selection of visible clouds had essentially zero possibility of VCCA omission errors. Snowfields and other unwanted bright features will be manually subtracted using the lasso tool to reduce VCCA commission errors. After the VCCA scores are established, the resulting cloud pixels will be filled with zeros and all others a value of one. The result will be a binary cloud mask that allowed a CC percentage computation serving as the cloud "truth" for validating the accuracy of the official HyCMA cloud mask.

7 References

Ackerman, S., K. I. Strabala, P. Menzel, R. Frey, C. C. Moeller, L. E. Gumley, B. Baum, S. W. Seemann, and H. Zhang (2006), Discriminating clear-sky from cloud with MODIS algorithm theoretical basis document (MOD35), *Cooperative Institute for Meteorological Satellite Studies, University of Wisconsin-Madison, NOAA/NESDIS, version 5.0, October 2006*.

Ackerman, S. A. (1996), Global satellite observations of negative brightness temperature differences between 11 and 6.7 mu m, *Journal of the Atmospheric Sciences*, *53*(19), 2803-2812.

Ackerman, S. A., K. I. Strabala, W. P. Menzel, R. A. Frey, C. C. Moeller, and L. E. Gumley (1998), Discriminating clear sky from clouds with MODIS, *Journal of Geophysical Research-Atmospheres*, *103*(D24), 32141-32157.

Ackerman, S. A., R. E. Holz, R. Frey, E. W. Eloranta, B. C. Maddux, and M. McGill (2008), Cloud detection with MODIS. Part II: Validation, *Journal of Atmospheric and Oceanic Technology*, *25*(7), 1073-1086.

Frey, R. A., S. A. Ackerman, Y. H. Liu, K. I. Strabala, H. Zhang, J. R. Key, and X. G. Wang (2008), Cloud detection with MODIS. Part I: Improvements in the MODIS cloud mask for collection 5, *Journal of Atmospheric and Oceanic Technology*, *25*(7), 1057-1072.

Hulley, G. C., and S. J. Hook (2008), A new methodology for cloud detection and classification with ASTER data, *Geophysical Research Letters*, *35*(16), L16812, doi: 16810.11029/12008gl034644.

Hutchison, K. D., and K. R. Hardy (1995), Threshold functions for automated cloud analyses of global meteorological satellite imagery, *International Journal of Remote Sensing*, *16*(18), 3665-3680.

Irish, R. R., J. L. Barker, S. N. Goward, and T. Arvidson (2006), Characterization of the Landsat-7 ETM+ automated cloud-cover assessment (ACCA) algorithm, *Photogrammetric Engineering and Remote Sensing*, *72*(10), 1179-1188.

Markham, B. L., and J. L. Barker (1986), Landsat MSS & TM Post-Calibration Dynamic Ranges, Exoatmospheric Reflectances & At-Satellite Temperatures*Rep.*

Rossow, W. B., and L. C. Garder (1993), Cloud Detection Using Satellite Measurements of Infrared and Visible Radiances for Isccp, *Journal of Climate*, *6*(12), 2341-2369.

Rossow, W. B., and E. N. Duenas (2004), The International Satellite Cloud Climatology Project (ISCCP) Web site - An online resource for research, *Bulletin of the American Meteorological Society*, *85*(2), 167-172.

Saunders, R. W., and K. T. Kriebel (1988), An Improved Method for Detecting Clear Sky and Cloudy Radiances from Avhrr Data, *International Journal of Remote Sensing*, *9*(1), 123-150.

Soden, B. J., and F. P. Bretherton (1993), Upper-Tropospheric Relative-Humidity from the Goes 6.7 Mu-M Channel - Method and Climatology for July 1987, *Journal of Geophysical Research-Atmospheres*, *98*(D9), 16669-16688.

Stowe, L. L. (1991), Cloud and Aerosol Products at Noaa Nesdis, *Global and Planetary Change*, *90*(1-3), 25-32.